J|A|C|S
ARTICLES
Published on Web 06/04/2002

Epitaxial Electrodeposition of Fe_3O_4 Thin Films on the Low-Index Planes of Gold

Thomas A. Sorenson,[†] Simon A. Morton,[‡] G. Dan Waddill,[‡] and Jay A. Switzer*,[†]

Contribution from the Department of Chemistry and Graduate Center for Materials Research, Department of Physics and Graduate Center for Materials Research, University of Missouri, Rolla, Rolla, Missouri 65409-1170

Received January 22, 2002

Abstract: Half-metallic ferrimagnetic materials such as Fe_3O_4 are of interest for use in spintronic devices. These devices exploit both the spin and charge of an electron in spin-dependent charge transport. Epitaxial thin films of Fe_3O_4 have been grown on the three low-index planes of gold by electrodeposition. On Au(110), a [110] Fe_3O_4 orientation that is aligned with the underlying Au(110) substrate is observed. Thin films on Au(100) grow with three different orientations: [100], [111], and [511]. On Au(111), both [111] and [511] orientations of Fe_3O_4 are observed. The [511] orientations are the result of twinning on {111} planes. A polarization value of approximately −40% at the Fermi level was measured by spin-polarized photoemission at room temperature for a thin film on Au(111).

Introduction

Spin-dependent charge transport is currently receiving a lot of attention due to potential applications in giant magnetoresistive (GMR) devices such as magnetic field sensors, magnetoresistive random access memories (MRAM), read heads, and galvanic isolators.[1,2] These devices require a source of spin-polarized electrons: a material in which the density of states at the Fermi level is different for spin-up and spin-down electrons. If the electrons of one spin are conducting whereas the electrons of the opposite spin are nonconductive, or 100% spin-polarized, the material is said to be half-metallic. Figure 1 illustrates a device based on the principle of spin-dependent charge transport. Two magnetic layers are separated by either a nonmagnetic layer or a thin insulating barrier. If half-metallic materials are used in these devices, when the spins are antiparallel, there is no available state in the layer of opposite spin to accept the electron. When the spins are parallel, the density of states in both layers are identical and electrons will flow across the barrier. Therefore, as the spin states of the two layers go from parallel to antiparallel, the resistance of the device increases. If the two magnetic layers are separated by a nonmagnetic layer, the device is called a spin valve, whereas if a thin insulating layer is used, the device is called a magnetic tunnel junction (MTJ). GMR effects are also observed across grain boundaries and interparticle contacts.

Magnetite, Fe_3O_4, is a promising source of spin-polarized carriers, because density-functional theory spin-resolved density of states calculations have suggested that electrons at the Fermi level are 100% spin-polarized.[3,4] Magnetite is a ferrimagnetic mixed-valence 3d transition metal oxide that has an inverse spinel structure (space group $Fd3m$) with a lattice constant of 0.8397 nm. The tetrahedral sites of the spinel structure are entirely occupied by Fe(III), whereas the octahedral sites are occupied half by Fe(II) and half by Fe(III). Fe_3O_4 undergoes a metal-to-insulator Verwey transition at 120 K, and the Curie temperature of magnetite is 860 K. The high Curie temperature

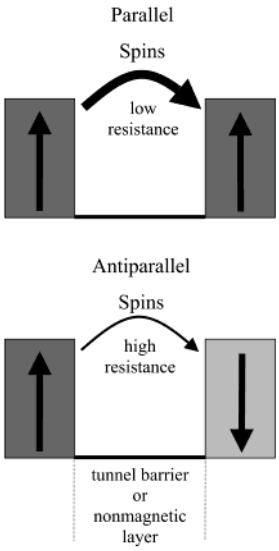

Figure 1. Schematic illustrating a device based on spin-dependent charge transport. A nonmagnetic or thin insulating layer separates two half-metallic magnetic layers. The resistance of the device increases as the spin states change from parallel to antiparallel.

* To whom correspondence should be addressed. E-mail: jswitzer@umr.edu.
[†] Department of Chemistry and Graduate Center for Materials Research.
[‡] Department of Physics and Graduate Center for Materials Research.

(1) Prinz, G. A. *Science* **1998**, *282*, 1660.
(2) Wolf, S. A.; Awschalom, D. D.; Buhrman, R. A.; Daughton, J. M.; von Molnar, S.; Roukes, M. L.; Chtchelkanova, A. Y.; Treger, D. M. *Science* **2001**, *294*, 1488.
(3) Zhang, Z.; Satpathy, S. *Phys. Rev. B* **1991**, *44*, 13319.
(4) Anisimov, V. I.; Elfimov, I. S.; Hamada, N.; Terakura, K. *Phys. Rev. B* **1996**, *54*, 4387.

10.1021/ja0201101 CCC: $22.00

is important for device applications. Recently, GMR effects greater than 500% have been reported at room temperature for Fe_3O_4 nanocontacts.[5]

Epitaxial thin films of Fe_3O_4 have been grown by MBE,[6−8] pulsed laser deposition,[9−11] laser ablation,[12−14] and oxidation of Fe thin films[15,16] on a variety of substrates. Our group has previously reported preliminarily results on the epitaxial electrodeposition of Fe_3O_4 on Au(111), a system with a 3% lattice mismatch.[17] Numerous other metal oxides, such as Bi_2O_3,[18,19] Cu_2O,[20] ZnO,[21−23] Tl_2O_3,[24] and PbO_2[25] have been epitaxially grown by electrodeposition on both metal and semiconductor substrates. In the present contribution, we expand on our previous study of Fe_3O_4 electrodeposition on Au(111),[17] report new results on Au(110) and Au(100), and present spin-polarized photoelectron measurements for Fe_3O_4 on Au(111).

Experimental Section

Preparation of Fe_3O_4 Thin Films. Thin films of Fe_3O_4 were prepared by oxidation of iron(II) using a bath first reported by Abe[26] via the reaction:

$$3Fe^{2+} + 4H_2O \leftrightharpoons Fe_3O_4 + 8H^+ + 2e^- \quad (1)$$

The $E°$ for the reverse of this reaction is +1.230 V vs NHE. The bath consisted of 0.04 M $K(CH_3COO)$ and 0.01 M $Fe(NH_4)_2(SO_4)_2{\cdot}6H_2O$. The pH of the solution was 6.5. The bath was kept at a constant temperature of 90 °C and purged with argon gas during deposition. At this pH and temperature, the calculated Nernst potential for the reaction is −0.43 V vs NHE (−0.63 vs Ag/AgCl). The thin films were grown by either applying a constant potential of −0.4 V vs Ag/AgCl(saturated KCl) or constant anodic current of 0.05 mA/cm^2 using an EG&G Princeton Applied Research model 273A potentiostat/galvanostat. Fe_3O_4 thin films can be grown at potentials of −0.45 to −0.30 V vs Ag/AgCl. Application of more positive potentials produces iron(III) oxide/hydroxide species. Gold single-crystal substrates with a diameter of 10 mm and a thickness of 2 mm were acquired from Monocrystal Company (Cleveland, OH). A gold wire was wrapped around the single crystals to secure the crystal and make electrical contact to the electrode during deposition. A gold wire was also used as the counter electrode.

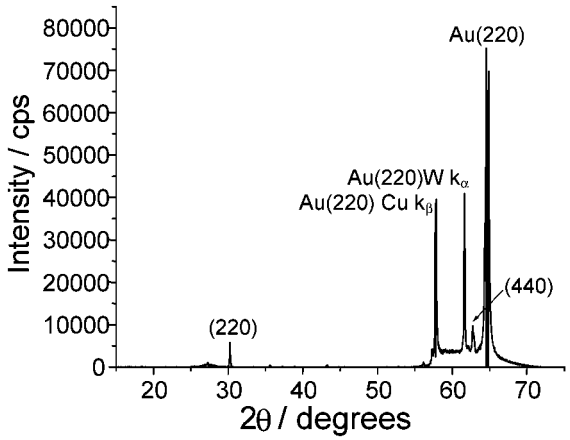

Figure 2. XRD pattern probing the out-of-plane orientation of a 400 nm Fe_3O_4 thin film electrodeposited on Au(110) at an anodic current density of 0.05 mA cm^{-2}.

X-ray Diffraction. X-ray diffraction (XRD) experiments for thin films on Au(110) and Au(100) were done with a Scintag XDA 2000 diffractometer using Cu Kα radiation. Texture analysis on the Scintag was done using a two-axis texture goniometer accessory that was fashioned in-house. XRD experiments for thin films on Au(111) were done using a Philips X'pert Pro Materials Research Diffractometer using Cu Kα_1 radiation. For $\theta-2\theta$ scans, a hybrid monochromator, consisting of a Göbel X-ray mirror and Ge[220] 2-bounce, 2-crystal monochromator, was used as the primary optic with a 0.18° thin film collimator as the secondary optic. The divergence of the hybrid monochromator is 25 arcseconds (0.007°). For texture analysis, a 2 mm × 2 mm cross-slit collimator with Ni filter was used as the primary optic, and a 0.27° parallel plate collimator with flat graphite monochromator was the secondary optic.

Spin Polarization. Spin-resolved photoelectron spectroscopy measurements were done for a thin film on Au(111) at the Advanced Light Source, Lawrence Berkeley National Laboratory, using Beamline 7.0.1 with the spin-resolved endstation.[27,28] The energy of the excitation beam was 158.8 eV. Emitted photoelectrons were collected and filtered by a PHI 10-360 SCA hemispherical electron energy analyzer and then passed into a micro-Mott detector to resolve the electron spins. The total energy resolution for the spin-resolved measurements was ∼0.5 eV. The sample was magnetized along the [110] direction parallel to the surface.

Results and Discussion

XRD Analysis of Fe_3O_4 Thin Film. Figure 2 shows $\theta-2\theta$ X-ray diffraction scan for a magnetite thin film grown on Au(110). The most predominant peaks besides those assigned to Au correspond to the (220) and (440) reflections of Fe_3O_4 at 2θ angles of 30.1° and 62.6°, respectively. Smaller peaks at 35.5°, 43.1°, and 57.0° are observed corresponding to the (311), (400), and (333) reflections of Fe_3O_4, respectively. In addition, an unknown broad peak centered at 27.5° is also observed.

To probe the in-plane orientation of the thin films, texture analysis has been used. The interplanar angles for all pole figures

(5) Versluijs, J. J.; Bari, M. A.; Coey, J. M. D. *Phys. Rev. Lett.* **2001**, *87*, 026601.
(6) Anderson, J. F.; Kuhn, M.; Diebold, U.; Shaw, K.; Stoyanov, P.; Lind, D. *Phys. Rev. B* **1997**, *56*, 9902.
(7) Shaw, K. A.; Lochner, E.; Lind, D. M. *J. Appl. Phys.* **2000**, *87*, 1727.
(8) Stanka, B.; Hebenstreit, W.; Diebold, U.; Chambers, S. A. *Surf. Sci.* **2000**, *448*, 49.
(9) Gong, G. Q.; Gupta, A.; Xiao, G.; Qian, W.; Dravid, V. P. *Phys. Rev. B* **1997**, *56*, 5096.
(10) Sena, S. P.; Lindley, R. A.; Blythe, H. J.; Sauer, C.; Al-Kafarji, M.; Gehring, G. A. *J. Magn. Magn. Mater.* **1997**, *176*, 111.
(11) Ogale, S. B.; Ghosh, K.; Pai, S. P.; Robson, M.; Li, E.; Jin, I.; Greene, R. L.; Ramesh, R.; Venkatesan, T.; Johnson, M. *Mater. Sci. Eng., B* **1998**, *56*, 134.
(12) Kennedy, R. J.; Stampe, P. A. *J. Phys. D: Appl. Phys.* **1999**, *32*, 16.
(13) Kleint, C. A.; Krause, M. K.; Hohne, R.; Lorenz, M.; Semmelhack, H. C.; Schneider, A.; Hesse, D.; Sieber, H.; Taubert, J.; Andra, W. *J. Phys. IV* **1997**, *7*, 593.
(14) Lindley, R. A.; Sena, S. P.; Blythe, H. J.; Gehring, G. A. *J. Phys. IV* **1997**, *7*, C1/617.
(15) Weiss, W.; Ritter, M. *Phys. Rev. B* **1999**, *59*, 5201.
(16) Kurtz, R. L.; Karunamuni, J.; Stockbauer, R. L. *Phys. Rev. B* **1999**, *60*, 16342.
(17) Nikiforov, M. P.; Vertegel, A.; Shumsky, M. G.; Switzer, J. A. *Adv. Mater.* **2000**, *12*, 1351.
(18) Bohannan, E. W.; Jaynes, C. C.; Shumsky, M. G.; Barton, J. K.; Switzer, J. A. *Solid State Ionics* **2000**, *131*, 97.
(19) Switzer, J. A.; Shumsky, M. G.; Bohannan, E. W. *Science* **1999**, *284*, 293.
(20) (a) Bohannan, E. W.; Shumsky, M. G.; Switzer, J. A. *Chem. Mater.* **1999**, *11*, 2289. (b) Switzer, J. A.; Kothari, H. M.; Bohannan, E. W. *J. Phys. Chem. B* **2002**, *106*, 4027.
(21) Liu, R.; Vertegel, A. A.; Bohannan, E. W.; Sorenson, T. A.; Switzer, J. A. *Chem. Mater.* **2001**, *13*, 508.
(22) Pauporte, T.; Lincot, D. *Electrochim. Acta* **2000**, *45*, 3345.
(23) Pauporte, T.; Lincot, D. *Appl. Phys. Lett.* **1999**, *75*, 3817.
(24) Vertegel, A. A.; Shumsky, M. G.; Switzer, J. A. *Electrochim. Acta* **2000**, *45*, 3233.
(25) Vertegel, A. A.; Bohannan, E. W.; Shumsky, M. G.; Switzer, J. A. *J. Electrochem. Soc.* **2001**, *148*, C253.
(26) Abe, M.; Tamura, Y. *Jpn. J. Appl. Phys.* **1983**, *22*, L511.
(27) Tobin, J. G.; Bedrossian, P. J.; Cummings, T. R.; Waddill, G. D.; S., M.; Larson, P.; Negri, R.; Peterson, E.; Boyd, P.; Gunion, R. *MRS Symp. Proc.* **1998**, *524*, 185.
(28) Denlinger, J. D.; Rotenberg, E.; Warwick, T.; Visser, G.; Nordgren, J.; Guo, J. H.; Skytt, P.; Kevan, S. D.; McCutcheon, K. S.; Shuh, D.; Bucher, J.; Edelstein, N.; Tobin, J. G.; Tonner, B. P. *Rev. Sci. Instrum.* **1995**, *66*, 1342.

Table 1. Interplanar Angles for a Cubic System

plane 1	plane 2	interplanar angle (deg)
(110)	(111), (11$\bar{1}$)	35.3
(100)	(311), (3$\bar{1}$1), (31$\bar{1}$), (3$\bar{1}\bar{1}$)	25.2
(111)	($\bar{3}$11), ($\bar{1}$13), (131)	29.5
(111)	($\bar{1}\bar{1}$3), ($\bar{1}$31), (13$\bar{1}$), (31$\bar{1}$), (1$\bar{1}$3), (3$\bar{1}$1)	58.5
(111)	($\bar{1}\bar{1}$3), (3$\bar{1}$1), ($\bar{1}$31)	80.0
(511)	(311)	9.45
(511)	(3$\bar{1}$1), (31$\bar{1}$)	29.5
(511)	(3$\bar{1}\bar{1}$)	41.0
(511)	(131), (113)	58.5
(511)	(13$\bar{1}$), (11$\bar{3}$)	66.0
(511)	(113), (1$\bar{3}$1)	80.0
(111)	(400), (040), (004)	54.7
(511)	(400)	15.8
(511)	(040), (004)	78.9

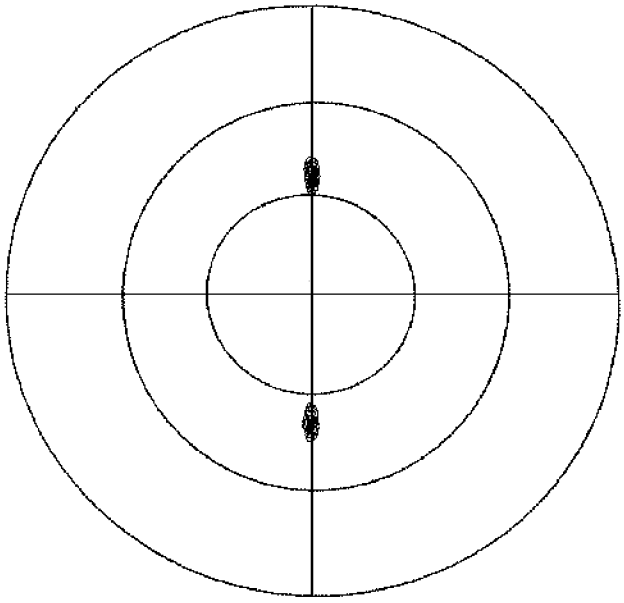

Figure 3. (111) X-ray pole figure of the Fe_3O_4 thin film on Au(110). The pole figure was obtained by setting 2θ to the angle for Fe_3O_4(111), 18.285°, and rotating the sample azimuthally, ϕ, from 0° to 359° for tilt angles, χ, from 0° to 60° in 1° increments. The radial grid lines on the pole figure correspond to 30° increments in the tilt angle, χ.

reported are presented in Table 1. The (111) pole figure for Fe_3O_4 on Au(110) is shown in Figure 3. The pole figure was acquired by setting 2θ equal to 18.285° and azimuthally rotating the sample from $\phi = 0°$ to 359°, at tilt angles, χ, from 0° to 60°. The only peaks that are observed in the pole figure appear at $\chi \cong 36°$. This agrees well with the angle between the (111) and (110) planes for cubic crystals of 35.3° as shown in Table 1. To establish the epitaxial relationship between the Fe_3O_4 and Au(110), (111) aximuthal ϕ scans for Au(110) were performed. The results indicate that both the {111} planes for Au(110) and the Fe_3O_4 thin film occur at the same ϕ angles, indicating that the Fe_3O_4 thin film is aligned with the Au(110) substrate.

On Au(100), peaks corresponding to the (111), (311), (222), (400), and (333) reflections are observed at 2θ angles of 18.3°, 35.4°, 37.2°, 43.0°, and 57.0°, respectively (Figure 4). It is of interest to note that the peak corresponding to the (333) peak is slightly larger in intensity than would be predicted based upon the heights of the (111) and (222) peaks. The intensities of the (111), (222), and (333) peaks are 10%, 8%, and 28%, respectively, for a powder XRD pattern according to PDF card file

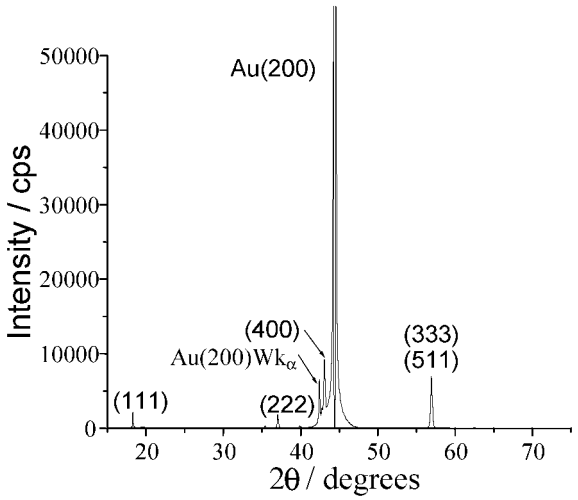

Figure 4. XRD pattern probing the out-of-plane orientation of a 450-nm Fe_3O_4 thin film electrodeposited on Au(100) at a constant potential of −0.40 V vs Ag/AgCl (sat'd KCl).

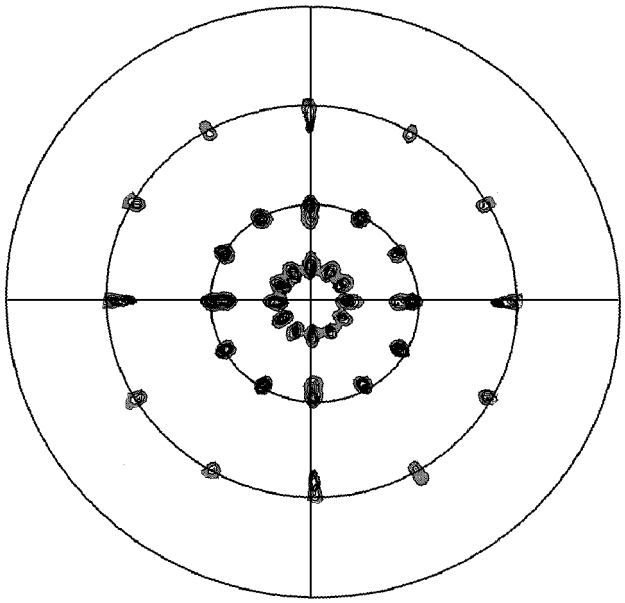

Figure 5. (311) X-ray pole figure of the Fe_3O_4 thin film on Au(100) for $\chi = 0°$ to 60°. The pole figure was obtained by setting 2θ to the angle for Fe_3O_4(311), 35.426° and rotating the sample as described in Figure 3. The radial grid lines on the pole figure correspond to 30° increments in the tilt angle, χ.

82−1533. The observed intensity ratio between the (111) and (333) is 1:3.2 rather than the predicted 1:2.8.

The pole figure for Fe_3O_4 on Au(100) is more complex (Figure 5) than the pole figure for Au(110). In this case, a (311) pole figure was acquired, as the (311) plane is the most intense scattering plane for Fe_3O_4. The pole figure from $\chi = 0°$ to 60° reveals 5 concentric rings of peaks at χ angles of 10°, 26°, 30°, 55°, and 59°. Assignment of the peaks at 26°, 30°,and 59° is uncomplicated: 25.2° is the interplanar angle between (311) and (100) while 29.5° and 58.5° are angles between (311) and (111) planes. The (100) peaks at 26° exhibit four-fold symmetry while the (111) peaks at 30° and 59° and exhibit 12-fold symmetry. (311) ϕ-scans of the Au(100) substrate show that the (100) peaks for the film are again aligned with the underlying Au(100) substrate. However, there is another ring of 12 peaks at $\chi \cong 10°$ that cannot be accounted for by either a [111] or

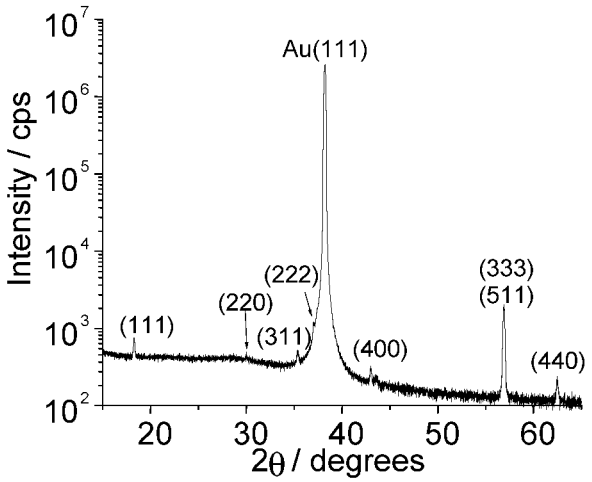

Figure 6. XRD pattern probing the out-of-plane orientation of a 775 nm Fe_3O_4 thin film electrodeposited on Au(111) at a constant potential of −0.40 V vs Ag/AgCl (sat′d KCl). The intensity has been plotted on the logarithmic scale.

[100] orientation. These peaks are assigned to (511) which would be expected to occur at an angle $\chi = 9.45°$. Evidence for a [511] orientation can also be found in the 2θ scan of Figure 4. As stated above, the (333) peak is larger than predicted on the basis of the intensity of the observed (111) and (222) peaks. As the (333) and (511) occur at the same 2θ angle, the larger than predicted intensity is indicative of the presence of (511). It should also be noted that those peaks in the pole figure assigned to (111) may also be due to (511) as shown in Table 1. For a (311) pole figure, every tilt angle in which a set of (111) peaks is observed, a set of (511) peaks exists as well. The Fe_3O_4 thin films appear to grow with three different orientations on Au(100): [100], [111], and [511]. Discussion on why we observe a [511] orientation will be presented below.

The $\theta-2\theta$ scan for an Fe_3O_4 thin film on Au(111) is shown in Figure 6 with the intensity plotted on a logarithmic scale. The most intense Fe_3O_4 peak observed corresponds to the (333) and (511) planes. Smaller intensity peaks corresponding to the (111), (220), (311), (222), (400), and (440) planes are also observed in the 2θ scan. Again, the (333) peak is much larger in intensity than predicted by the powder pattern and the (111) peak height, in this case the ratio is 1:5.8 rather than the predicted ratio of 1:2.8. The (311) and (400) pole figures for Fe_3O_4 on Au(111) are shown in Figure 7 for tilt angles, χ, from 0° to 85°. Six rings of peaks are observed in the (311) pole figure (Figure 7a) corresponding to $\chi \cong 10°$, 29°, 40°, 59°, 67°, and 80°. Examination of the interplanar angles in Table 1 shows that the observed peaks at 10°, 40°, and 67° are due to [511] orientations. The remaining rings of peaks at 29°, 59°, and 80° could be due to either [511] or [111] orientations. No in-plane orientations for any of the other peaks present in the $\theta-2\theta$ scan (Figure 6) are observed in the pole figure.

Given the small intensity of the (111) and (222) peaks in Figure 6, the (400) pole figure is shown in Figure 7b to demonstrate that there is a [111] in-plane orientation. There are three rings of peaks in this pole figure at $\chi \cong 16°$, 55°, and 79°. The peaks at 16° and 79° are due to [511] orientations. The six peaks at 55° are at the correct tilt angle for a parallel and antiparallel [111] orientation, however, three of the peaks are 10× more intense than the other three. The three large

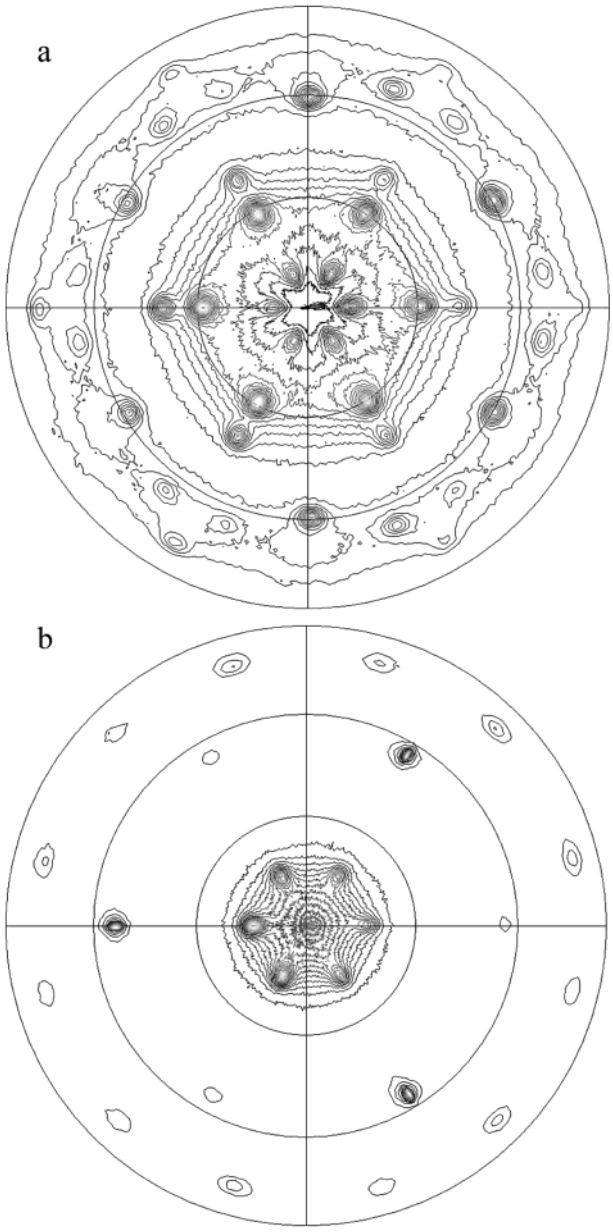

Figure 7. X-ray pole figures for the Fe_3O_4 thin film electrodeposited on Au(111). (a) (311) pole figure for $\chi = 0°$ to 85°. (b) (400) pole figure for $\chi = 0°$ to 85°. The radial grid lines on the pole figure correspond to 30° increments in the tilt angle, χ.

intensity peaks at 55° are actually due to {200} planes of the Au(111) substrate. The 2θ angle for the (400) peak of Fe_3O_4 used in this pole figure is 43.054° while the 2θ angle for the (200) peak of Au is 44.392°. While the measured fwhm of the Au(111) peak in Figure 6 is 0.187° (the *y*-axis of Figure 6. is plotted on the log scale), at the baseline, the width of the Au-(111) peak is about 4°. Due to the significantly lower intensity of the Fe_3O_4 peaks compared to the Au peak, as demonstrated by the peak heights in Figure 6, the three large intensity peaks at $\chi \cong 55°$ are due to the low-angle tail of the Au(200) peak at 44.392°. This was confirmed by tilting and rotating the sample to the χ and ϕ angles of a large peak and a small peak and running a $\theta-2\theta$ scan; the large peak was centered at 44.4°, whereas the small peak was centered at 43.1°. The smaller peaks correspond to an antiparallel [111] orientation of Fe_3O_4 on Au-

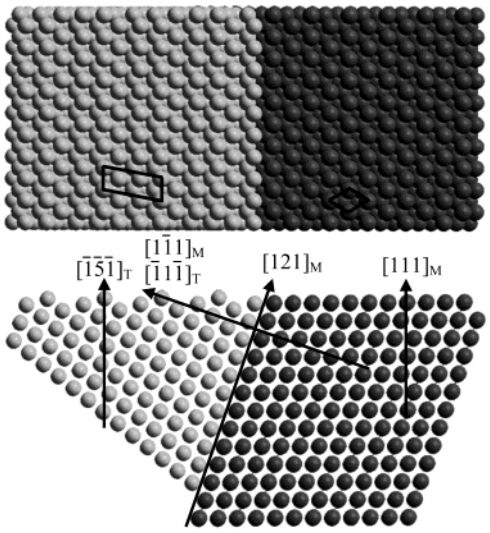

Figure 8. Side and top view model showing twinning of two face-centered cubic crystallites along {111} planes. The matrix (M) is shown on the right (dark) and the twin (T) is shown on the left (light). Twinning the $[111]_M$ oriented crystallite along the $(1\bar{1}1)$ results in a $[\bar{1}5\bar{1}]_T$oriented twinned crystallite. The top view shows the $(111)_M$ and $(\bar{1}5\bar{1})_T$ unit meshes.

(111) because the peaks for the (400) orientation are rotated 60° from the (200) peaks of Au. However, the (400) peaks that would be observed for a parallel [111] orientation of Fe_3O_4 are obscured by the larger (200) peaks of Au. It is not possible from these pole figures to determine the relative amounts of the parallel and antiparallel orientations.

Twinning of {111} Planes Resulting in ⟨511⟩ Orientations. Summarizing thus far, on all three low index planes of Au, we observed orientations of Fe_3O_4 that follow the substrate. However, on Au(100) and Au(111), additional orientations are present, in particular [511] orientations. These [511] orientations observed are the result of twinning on {111} planes. Twinning can be described by the matrix, $T_{(hkl)}$, by the relationship

$$(PQR) = T_{(hkl)}(pqr) \tag{2}$$

where *(PQR)* is a lattice plane in the twinned crystallite that corresponds to the lattice plane, *(pqr)*, of the original crystallite after twinning on *(hkl)*.[29,30] The general twin matrix for cubic systems is

$$T_{(hkl)} = \frac{1}{(h^2+k^2+l^2)} \begin{pmatrix} h^2-k^2-l^2 & 2hk & 2hl \\ 2hk & -h^2+k^2-l^2 & 2kl \\ 2hl & 2kl & -h^2-k^2+l^2 \end{pmatrix} \tag{3}$$

In face-centered cubic crystal structures, twinning occurs on {111} planes and the twinning matrix takes the form

$$T_{\langle 111\rangle} = \frac{1}{3}\begin{pmatrix} -1 & 2hk & 2hl \\ 2hk & -1 & 2kl \\ 2hl & 2kl & -1 \end{pmatrix} \tag{4}$$

If twinning occurs on the $(1\bar{1}1)$, as illustrated in Figure 8, the twinning matrix becomes

$$T_{(1\bar{1}1)} = \frac{1}{3}\begin{pmatrix} -1 & -2 & 2 \\ -2 & -1 & -2 \\ 2 & -2 & -1 \end{pmatrix} \tag{5}$$

To determine the direction in the twinned crystal that is parallel to the original [111] growth direction (assuming that the thin film starts with the [111] orientation of the substrate) after twinning on the $(1\bar{1}1)$, eq 2 is solved using the matrix shown in eq 5 with $(pqr) = (111)$, resulting in $(PQR) = 1/3\ (\bar{1}5\bar{1})$. The $[\bar{1}5\bar{1}]$ direction of the twinned crystallite is parallel to [111] of the original crystallite. Twinning of {111} planes resulting in ⟨511⟩ orientations has been previously reported in thin films of fcc metals.[31−33] *Dana's Manual of Mineralogy* reports that magnetite crystals are occasionally found twinned on {111} planes according to a rule commonly referred to as the spinel twin law.[34] Also, a TEM study of nanoscale magnetite crystallites formed either synthetically or biogenically by bacteria reported crystallites highly twinned along {111} planes according to the spinel twin law.[35]

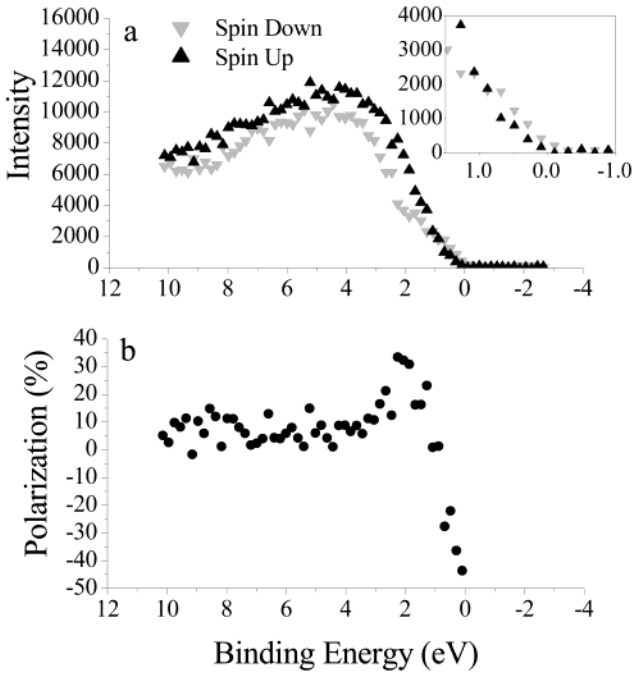

Figure 9. Spin-polarized photoemission results for an electrodeposited Fe_3O_4 thin film on Au(111). (a) photoelectron intensity for spin-up and spin-down electrons as a function of binding energy. The inset shows the measured photoelectron intensity around 0 eV binding energy. (b) polarization curve calculated from (a).

Spin-Polarization Measurements. Spin-polarization photoemission results at room temperature for an Fe_3O_4 thin film on Au(111) are shown in Figure 9. In this measurement, a 158.8 eV excitation beam is used to elastically eject valence band electrons from the thin film into vacuum using the photoelectric effect. The photoelectrons are then separated on the basis of kinetic energy using a hemispherical electron energy analyzer

(29) Andrews, K. W.; Johnson, W. *Br. J. Appl. Phys.* **1955**, *6*, 92.
(30) Thomas, G.; Goringe, M. J. *Transmission Electron Microscopy of Materials*; John Wiley & Sons: New York, 1979; p 95.
(31) Zeng, Y.; Zou, Y. L.; Alford, T. L. *Thin Solid Films* **1997**, *307*, 89.
(32) Tomov, I.; Adamik, M.; Barna, P. B. *Thin Solid Films* **2000**, *371*, 17.
(33) Rashkov, S.; Stoichev, D. S.; Tomov, I. *Electrochim. Acta* **1972**, *17*, 1995.
(34) Hurlbut, C. S. J. In *Dana's Manual of Mineralogy*; John Wiley & Sons: New York, 1971; p 295.
(35) Devouard, B.; Posfai, M.; Hua, X.; Bazlinski, D. A.; Frankel, R. B.; Buseck, P. R. *Am. Mineral.* **1998**, *83*, 1387.

and sent into a micro-Mott detector. The micro-Mott detector determines the distribution of spin-up and spin-down electrons from the surface of the magnetite thin film.[36]

The measured intensity of spin-up and spin-down electrons is shown in Figure 9a with the corresponding values for polarization in Figure 9b. No attempt was made to clean the surface by either ion bombarding or annealing as prior attempts to clean the surface in this manner resulted in either a marked decrease or loss of magnetism at the surface of the thin film. From the plot in Figure 9a, the polarization percentage, P, is calculated by the equation:

$$P = \frac{I(\uparrow) - I(\downarrow)}{I(\uparrow) + I(\downarrow)} \times 100\% \quad (6)$$

where $I(\uparrow)$ and $I(\downarrow)$are the measured intensities of spin-up and spin-down electrons, respectively. At the Fermi level, the measured polarization at room temperature is approximately −40%. This measured polarization is short of the calculated polarization of 100%.[3] A polarization value of −40% and the shape of the polarization curve are both comparable with measured photoelectron spin-polarization from a single-crystal Fe_3O_4 sample at 10 K.[37]

There are a number of possible explanations for not observing 100% spin polarization. First, photoemission experiments are surface techniques and only probe the upper few nanometers of the material. X-ray photoelectron spectroscopy has shown that the surface of our sample is covered with an adventitious carbon layer inherent in ex situ surface analysis measurements. Another possibility is that the surface layer of Fe_3O_4 is not a true truncation of the bulk but is reconstructed or terminated with only one type of iron ions, as is frequently observed for clean metal oxide surfaces.[38] The surface could therefore have different magnetic properties than the bulk of the material. Differing magnetization at the surface has been used to explain measured spin-polarization values of ∼40% for a 60-nm thick thin films of another predicted half-metallic compound, NiMnSb.[39,40] In addition, in these experiments the Fermi level is taken to be the threshold energy for photoemission. The exact location of the Fermi level is somewhat uncertain due to the low signal-to-noise ratio at the threshold energy. The spin polarization is determined from the difference between the two very small signals at the threshold energy, and is, therefore, also subject to error. Finally, it may be that the calculations of 100% spin polarization need to be reevaluated.

Nonetheless, even if the measured room-temperature polarization value of −40% is correct, magnetoresistive devices can still be fabricated from Fe_3O_4. As stated in the Introduction, room-temperature magnetoresistance values of over 500% have been reported for Fe_3O_4 nanocontacts.[5] Electrodeposition holds a distinct advantage over many other deposition techniques in that high processing temperatures are not required. There is, for example, much interest in combining magnetoresistive devices with traditional semiconductors.[41] The low processing temperature makes electrodeposition an advantageous deposition technique for growing thin films on substrates such as Si, GaAs, and InP.

Conclusions

Thin films of Fe_3O_4 have been deposited on Au single-crystal substrate by anodic electrodeposition from a solution of Fe(II) ions at 90 °C. A [110] Fe_3O_4 orientation is observed for deposition on Au(110). On Au(100) three orientations, [100], [111], and [511], for magnetite thin films are observed. Thin films on Au(111) single crystals had both [111] and [511] orientations. The [511] orientations on Au(111) and Au(100) are the result of twinning on {111} planes. A spin polarization of approximately −40% was measured at room temperature by spin-polarized photoemission for an epitaxial thin film of Fe_3O_4 on Au(111).

Acknowledgment. The National Science Foundation (CHE 9816484, DMR 0071365, and DMR 0076338) and the Foundation for Chemical Research are gratefully acknowledged for financial support of this work. The Advanced Light Source is supported by the Director, Office of Science, Office of Basic Energy Sciences, Materials Sciences Division, of the U.S. Department of Energy under Contract No. DE-AC03-76SF00098 at Lawrence Berkeley National Laboratory.

JA0201101

(36) Johnson, P. D. *Rep. Prog. Phys.* **1997**, *60*, 1217.
(37) Alvarado, S. F.; Eib, W.; Meier, F.; Pierce, D. T.; Sattler, K.; Siegmann, H. C.; Remeika, J. P. *Phys. Rev. Lett.* **1975**, *34*, 319.
(38) Freund, H. J.; Kuhlenbeck, H.; Staemmler, V. *Rep. Prog. Phys.* **1996**, *59*, 283.
(39) Zhu, W.; Sinkovic, B.; Vescovo, E.; Tanaka, C.; Moodera, J. S. *Phys. Rev. B* **2001**, *64*, 060403.
(40) de Wijs, G. A.; de Groot, R. A. *Phys. Rev. B* **2001**, *64*, 020402.
(41) Prinz, G. A. *Science* **1990**, *250*, 1092.